Supplementary Material (ESI) for Molecular BioSystems

STRUCTURE OF THE EGF RECEPTOR TRANSACTIVATION CIRCUIT INTEGRATES MULTIPLE SIGNALS WITH CELL CONTEXT

Elizabeth J. Joslin[1], Harish Shankaran[2], Lee K. Opresko[2], Nikki Bollinger[2], Douglas A. Lauffenburger[1], and H. Steven Wiley[2,3]

[1]Department of Biological Engineering, Massachusetts Institute of Technology, Cambridge, MA, 02139. [2]Systems Biology Program and [3]Environmental Molecular Sciences Laboratory, Pacific Northwest National Laboratory, Richland, WA 9354.

SUPPLEMENTAL MATERIAL

Contents:

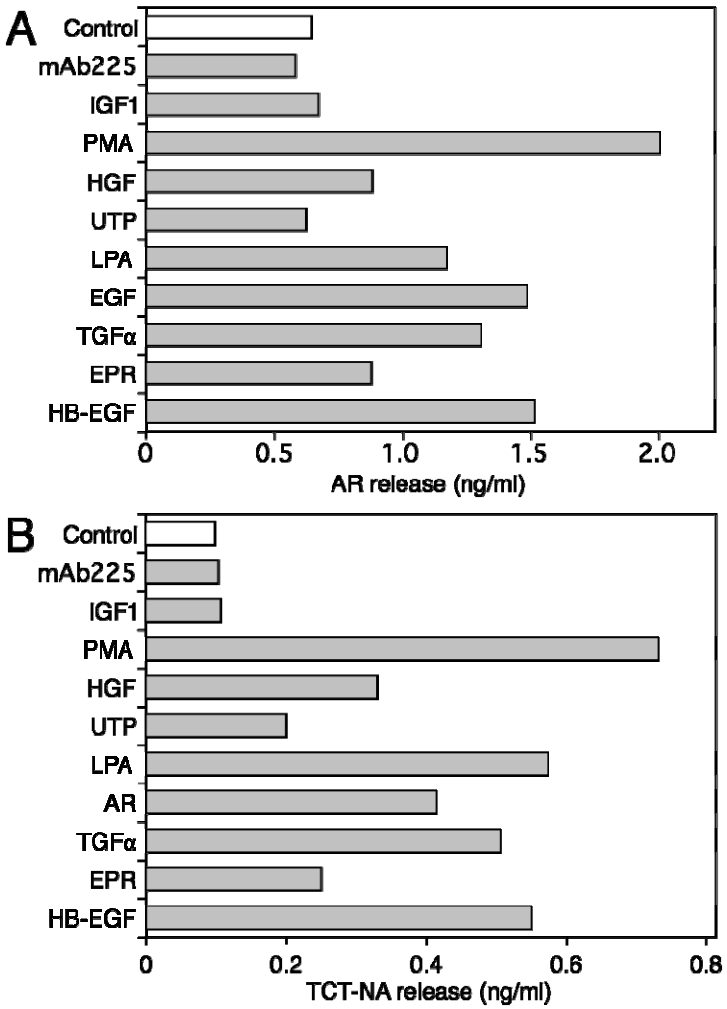

Supplementary Figure S1. The ability of different agonists to stimulate TCT-NA shedding is the same as observed for autocrine amphiregulin

(**A**) HMEC were plated at a density of 320,000 cells per well in 6-well dishes. After 48hrs, cells were switched to serum-free medium (control) or medium including 225 mAb (10μg/ml), IGF1 (3nM), PMA (1μM), HGF (20ng/ml), UTP (100μM), LPA (5μM), EGF (10ng/ml), TGFa (10ng/ml), EPR (20ng/ml) or HB-EGF (40ng/ml). After 2 hr, the medium was collected and the concentration of amphiregulin was determined by ELISA.

(**B**) Identical to panel **A**, except that cells expressing TCT-NA were used instead and the ELISA was specific for EGF. AR (100ng/ml) was substituted for EGF in the panel of stimulants.

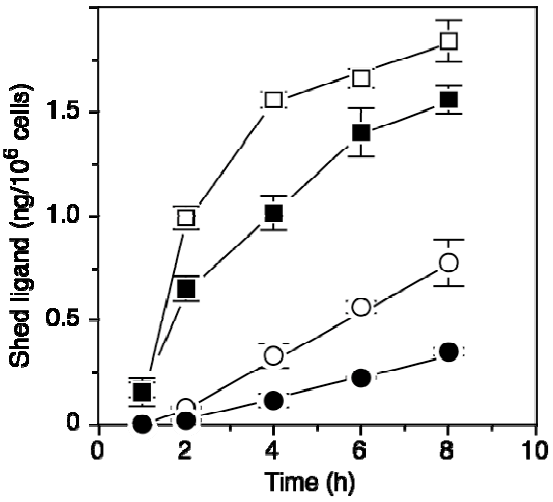

Supplementary Figure S2. Stimulated shedding of TCT-NA is weakly dependent on p38
After 16 hours in serum-free media, TCT cells were pre-incubated either with (closed symbols) or without (open symbols) 10 μM SB203580 for 30 minutes. At t=0 cells were switched to fresh serum-free media alone (circles) or media containing 20 ng/ml TGF (squares) both with and without 10 μM SB203580. Media was collected at indicated intervals and EGF concentrations were measured by ELISA. Error bars are SD from triplicate wells.

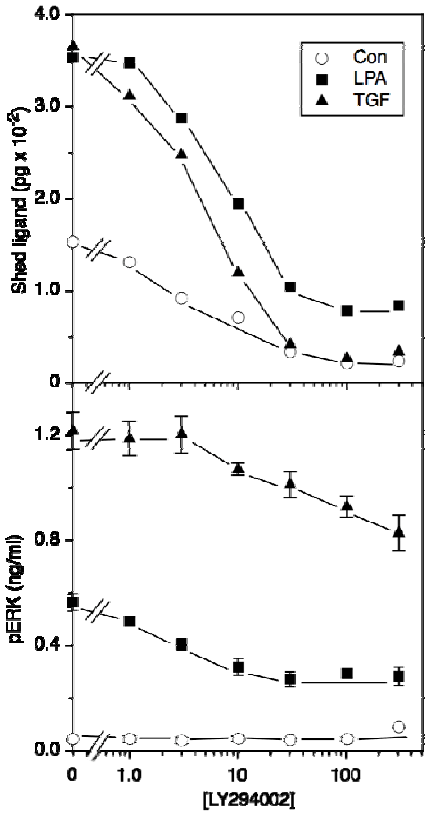

Supplementary Figure S3. Effect of PI3K inhibition on both TGF and LPA-stimulated shedding and ERK phosphorylation

(**A**) Cells expressing TCT-NA (700K per well) were changed to serum-free medium overnight before a 1 hour treatment with in the indicated concentration of LY294002. LPA (0.5 μM) or TGF (2.5 ng/ml) was added in a small aliquot (20μL) and the cells incubated for an additional hour prior to collecting the medium and measuring the level of immunoreactive EGF by ELISA. The data is the average of duplicate wells.

(**B**) Same as panel **A**, but using HMEC at 500K per well. At 15 min following agonist treatment, cells were rinsed in ice-cold saline and lysed in detergent as described in Methods. The levels of phospho-ERK were then measured by ELISA.

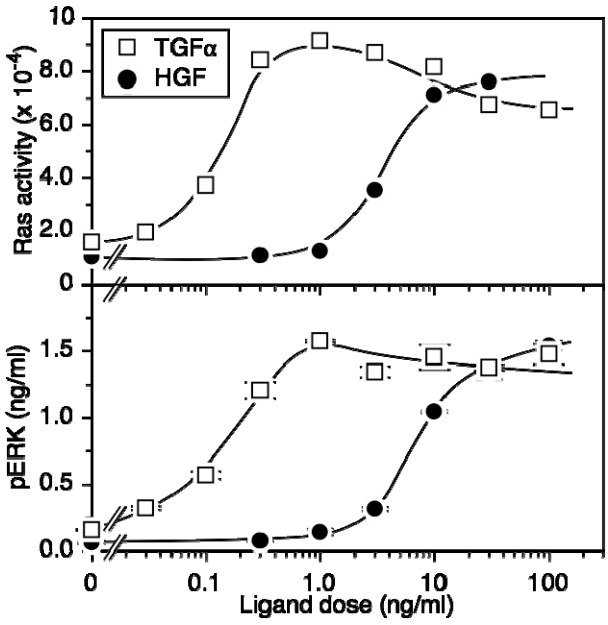

Supplementary Figure S4. The relationship between HGF and TGF concentrations and the levels activated Ras and phospho-ERK
Cells were plated at a density of ~6 x 10^6 cells in 150 cm dishes, grown for 48hr and then changed to serum-free medium overnight. Half of the cells were treated with 10µg/ml 225 mAb for 1 hour and then treated with the indicated concentrations of HGF (closed circles). The other cells were treated with the indicated concentrations of TGF (open squares). After 5 min, all cells were rinsed and lysed with detergent using the protocol for the Ras assay as outlined in the Methods. The cell lysates were used for both determining the levels of Ras and phospho-ERK as outlined in the Methods.

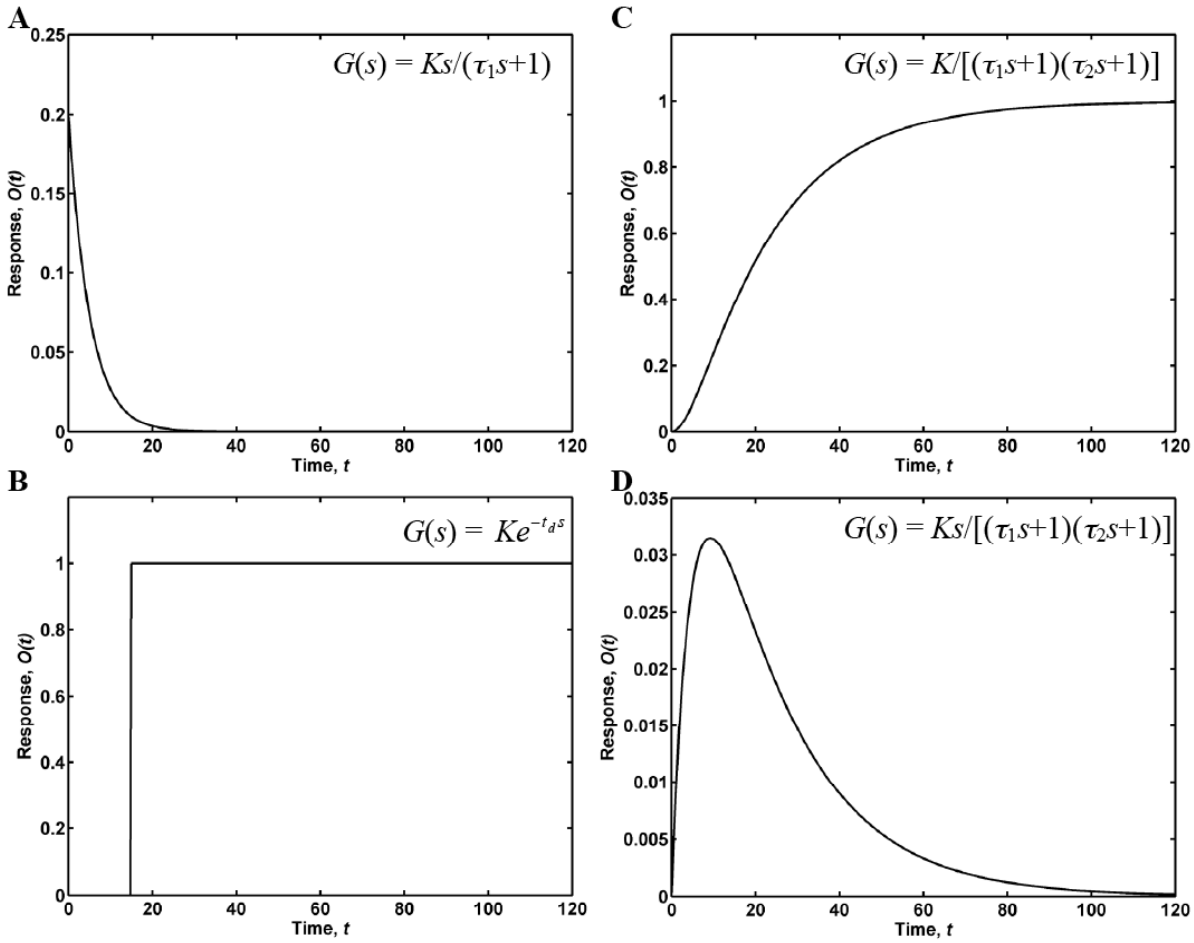

Supplementary Figure S5. Unit step response of transfer function types used in the mathematical model

The transfer function forms and the module(s) that they are used for are as follows: (**A**) $G(s) = Ks/(\tau_1 s+1)$ – module 1, (**B**) $G(s) = Ke^{-t_d s}$ – module 2, C) $G(s) = K/(\tau_1 s+1)(\tau_2 s+1)$ – module 3 D) $G(s) = Ks/(\tau_1 s+1)(\tau_2 s+1)$ – modules 4 and 5. Results are shown for the following parameter values: $K = 1$, $\tau_1 = 5$, $\tau_2 = 20$, $t_d = 15$ mins.

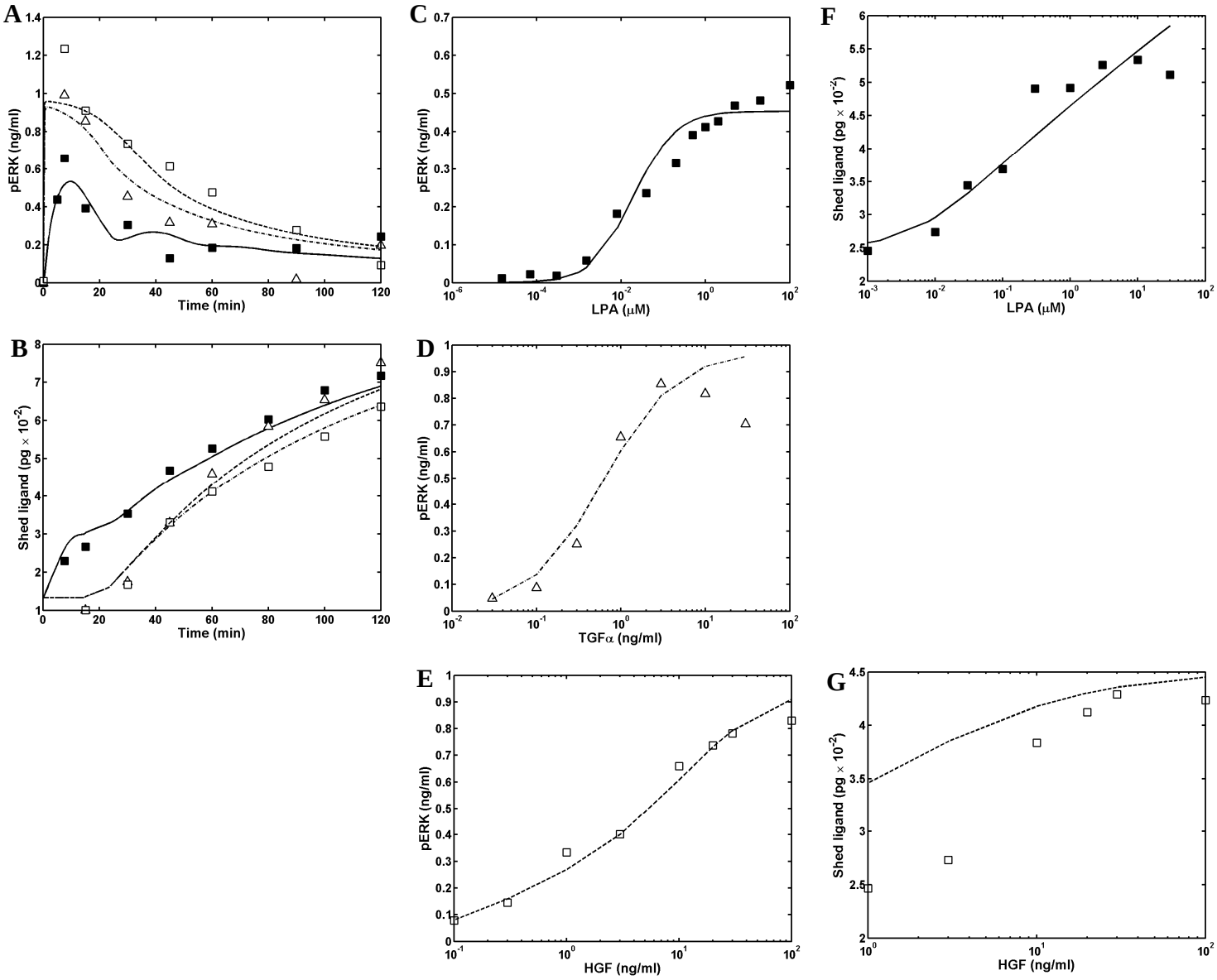

Supplementary Figure S6. Model fits to the experimental data.
Model fits (lines) to experimental data (markers) are shown for pERK (panel A) and ligand shedding (panel B) time courses in response to fixed concentrations of LPA, TGF and HGF; the pERK response to varying doses of LPA (panel C), TGF (panel D) and HGF (panel E); and the ligand shedding response to varying doses of LPA (panel F) and HGF (panel G). The conditions under which the experiments were done are described in the corresponding figures in the main manuscript. The marker shapes that are used are the same as those in Fig. 2A and 2C of the manuscript: LPA addition experiments are denoted by filled squares, HGF addition by open squares and TGF addition by open triangles. Model fits for these respective input conditions are denoted using solid lines, dashed lines and dash-dot lines. The R^2 values for the 11 different curves are as follows: Panel A – L-E: 0.813, T-E: 0.917, H-E: 0.909; Panel B – L-S: 0.983, T-S: 0.941, H-S: 0.947; Panel C – L-E: 0.951; Panel D – T-E: 0.908; Panel E – H-E: 0.984; Panel F – L-S: 0.874, Panel G – H-S: 0.474. Here, the curve corresponding to each R^2 value is identified by specifying the input, *I* (L=LPA, T=TGF, H=HGF) and output, *O* (E=ERK and S=Shed ligand) in the form *I-O*.

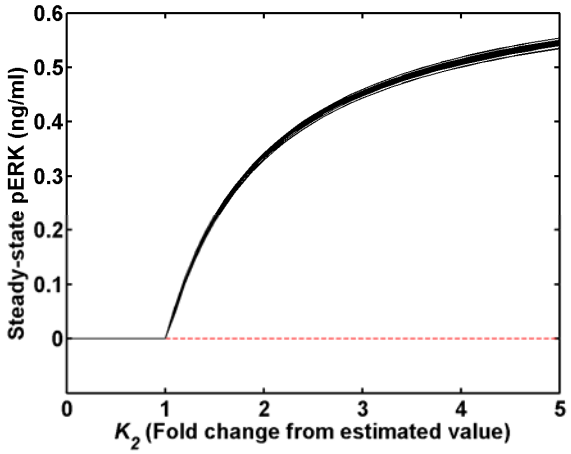

Supplementary Figure S7. Model predictions for system steady-state using alternate solution sets obtained during parameter estimation.
For each parameter set, steady-state pERK levels were computed for the autocrine feedback loop, and are plotted as function of the fold change of K_2 from its actual value in the parameter set. K_2 is the gain of the ERK-induced shedding module. The stable steady state is depicted using a solid black line. The red line indicates the unstable steady state at pERK = 0. Results are shown for the 10 best parameter estimates determined based on the root-mean-squared deviation between model predictions and experimental data. As seen, predictions using the various parameter estimates are in excellent agreement with each other. Thus, despite the uncertainty in the absolute values of certain parameters (Table S3), our results regarding the behavior of the autocrine system (Fig. 8 of the manuscript) would remain essentially unchanged.

SUPPLEMENTARY METHODS: COMPUTATIONAL MODELING OF EGFR TRANSACTIVATION DYNAMICS

Mathematical model description and assumptions

Module-based approaches where a biological network is partitioned into functional modules at a coarse-grained level are being increasingly applied to understand biological systems [1-4]. For system-level analysis of a modular network, each module can be treated as a proverbial 'black box' whose internal mechanisms do not have to be explicitly represented or even known. Molecular interactions within a module are only important with respect to their effect on how the module converts an input to an output; they can otherwise be ignored in analyzing the system properties. A modular network model is thus a natural choice for the EGFR transactivation circuit where details of the molecular mechanisms are unknown, but the coarse-grained modular structure of the network has been established.

We developed a block diagram representation for the transactivation system based on the network structure deduced in the manuscript (Fig 7). We defined the system as containing five distinct Linear Time-Invariant (LTI) modules (modules 1-5 in Fig. 7) that are involved in converting the three inputs (LPA, TGFα and HGF concentration time-series) to the levels of ligand shedding rate and ERK activation. The input-output dynamics of these modules are described using transfer functions (TFs). There are two distinct classes of processes in this system – ligand shedding and ERK activation. We chose two distinct ligand shedding modules: i) an *LPA induced shedding* module with input being the LPA concentration profile, ii) an *ERK induced shedding* module with input being the level of phosphorylated ERK. The outputs of each of these modules is a *shedding rate* and the overall ligand shedding rate, is the sum of these outputs. We chose three distinct ERK activation modules: i) an *autocrine ligand induced ERK* module with input being the ligand shedding rate, ii) a *TGFα induced shedding* module with input being the TGFα concentration profile, iii) a *HGF induced shedding* module with input being the HGF concentration profile. The output of each of these modules is the level of phosphorylated ERK (pERK), and the overall pERK level is the sum of these outputs. In order to make the model realistic, we assumed that the net ligand shedding rate and ERK activity are each saturable. We filtered the additive outputs of the LTI ligand shedding modules, and ERK activation modules using static (memoryless) sigmoidal functions (modules 6 and 7 respectively in Fig. 7). Thus, saturation of the ligand shedding rate and ERK activation are assumed to be inherent properties of these processes themselves, and are considered to be independent of the type of stimuli that activate these processes. Finally, we integrated the filtered ligand shedding

rate to obtain the absolute shed amount at any given time. All of the model variables are treated as deviations in the output levels from their respective values in the control experiment.

Core modules 2 and 3 together describe an autocrine positive feedback loop, and the system inputs feed into this loop by contributing independently to either ligand shedding (LPA) or ERK activation (TGFα and HGF). Our objective is to deduce the input-output relationships of the system modules from the closed loop system responses measured in our experiments. Information about the input-output behavior of the LTI modules is available from the dynamics experiments where LPA, TGFα and HGF are each used as the system inputs (Figs. 2A and 2C), while information about shedding and p-ERK saturation is available from dose response experiments using LPA, TGFα and HGF individually (Figs. 4A, 4B, 6C and 6D). Our approach is to simultaneously fit the model to all of the data from these experiments to determine the model parameters. The implicit assumption here is that the dynamics and saturation properties of the feedback loop itself remain unchanged under these different input conditions.

Another assumption in our analysis is that the five ERK activation and ligand shedding modules are treated as LTI systems. The assumption of linearity for modules 2 and 3 are supported by our experimental observations. Although LPA-induced shedding, TGF -induced pERK, and HGF-induced pERK have large linear regimes, they are nonlinear for high values of the input strength (see the dose response data). We account for these nonlinearities by modeling ligand shedding and ERK activation as saturable processes. However, since we only have time course measurements at a single ligand dose for each of the stimuli, we make the simplifying assumption that the shape of the time course does not change with input strength for modules 1, 4 and 5. The assumption of linearity does not restrict our ability to capture the dynamics experiments in Fig. 2 since linear systems are capable of generating a wide variety of input-output dynamics through the combination of multiple exponential functions in the time domain. Mathematical functions derived from linear dynamic systems would be sufficiently complex to capture the input-output time course relationships seen in this system.

The inputs to the model are the time-dependent concentrations of LPA, TGF and HGF. The outputs are the time dependent levels of pERK, $y_7(t)$ and shed ligand, $y_8(t)$ (Fig. 6) . We assume that the inputs are step functions, i.e. the ligand concentration increases to the specified dose at time 0, and stays at this value. Given the input doses of LPA, TGF and HGF, the model predicts the time courses of ERK activation and ligand shedding. The development of the mathematical model - our specific choices for the transfer function forms for modules 1-5 – and parameter estimation procedures for the entire model are detailed below.

Transfer functions for modules 1 to 5, and interpretation of their functional forms

For a linear system, the output, $O(t)$, in the time domain can be obtained by convoluting its unit impulse response, $G(t)$ with the input, $I(t)$. $G(t)$, is the system output when the input is a single sharp pulse at t=0 with an area under the integral of 1. The input-output relationship can be written in the time-domain as:

$$O(t) = \int_0^t G(t-\tau)I(\tau)d\tau \qquad \text{(S1)}$$

This relationship can be expressed in a more convenient algebraic form by taking the Laplace transform of Eq. S1, which yields $O(s) = G(s)I(s)$. $G(s)$ is known as the transfer function (TF) of the system. Note that for a unit impulse input, the Laplace transform of the input $I(s) = 1$, and hence $O(s) = G(s)$; i.e., when the input is a unit impulse, the output is given by $G(s)$.

The functional form of $G(s)$ encodes the qualitative characteristics of the system response. For instance when the TF is a constant, i.e. $G(s) = K$, we have a simple gain system with the shape of the output time-series being identical to that of the input. For $G(s) = K/(\tau s+1)$, the impulse response in the time domain is *an instantaneous rise* from 0 to a maximum value, followed by an exponential decay with rate $1/\tau$ and half-life $\tau \log_e 2$; this is called a first-order system. For $G(s) = K/(\tau_1 s+1)(\tau_2 s+1)$, the impulse response is a rise from zero at t=0 to a maximum value in a *finite amount of time*, followed by a decay to zero; this is a second-order system. The overall response decay time is controlled by the larger of the two time constants, τ_1 and τ_2. For $G(s) = Ke^{-t_d s}$, the output profile mirrors that of the input after a dead-time of t_d where the output does not change; we refer to this as a system with dead-time. From a practical standpoint, the K in the numerator of the aforementioned TFs is the gain of the system and specifies how the system amplifies (attenuates) the input. The τ values in the denominator are time constants, which specify the lag between the input and output, i.e. the sluggishness of the response. The t_d value in a term of type $e^{-t_d s}$ in the numerator specifies the dead-time.

An 's' term in the numerator of the TF amounts to taking the derivative of the input. In our experiments the inputs are step changes in the ligand concentration. A unit step change input has a laplace transform $I(s) = 1/s$. An 's' term in the numerator of the TF, converts this input to an impulse. For instance, when $G(s) = Ks/(\tau s+1)$, the output in response to a step input is $O(s) = G(s)\times I(s) = Ks/(\tau s+1) \times 1/s = K/(\tau s+1)$. This output in the time domain would be an *instantaneous rise* from 0 to a maximum value, followed by an exponential decay with rate $1/\tau$.

Note that the output would decay to 0 even though the input remains at a constant non-zero value. Thus, the output 'adapts' to the constant presence of a stimulus and returns to its original value. When $G(s) = Ks/(\tau_1 s+1)(\tau_2 s+1)$, we again have an adaptive response, but the output in response to a step input would be a rise to a maximum value in a *finite amount of time*, and would eventually decay to zero.

Transfer function forms chosen for the five system modules

In conceptual terms, we have a system identification problem where we need to determine the transfer function forms for the modules as well as their parameters from the measured input and output time-series. This problem can be posed as a non-linear optimization where the error between the model predictions for the output time-series and the experimental output time-series is minimized by adjusting the model functions and parameters. Although this is conceptually simple, non-linear optimization has pitfalls. Inclusion of too many parameters can result in multiple optima, make parameter estimation unreliable, and complicate the interpretation of the results. Thus, automatically identifying a form for the module transfer functions as part of the optimization would complicate the data analysis. As an alternative, we chose to specify the simplest possible transfer function forms for each of the modules based on the qualitative dynamic features of the EGFR transactivation circuit. The optimization problem is then reduced to the task of determining the TF parameters alone. The TF forms chosen for the five system modules and the rationale for their selection are provided in Table S2. The step response encoded by these TF forms is shown in Fig. S5.

Governing equations for the mathematical model

Transfer functions are a concise way to represent the solution of linear ordinary differential equations (ODEs). Each of the five LTI modules can be described by a particular ODE which when solved yields its transfer function. Note that a first-order system (module 1) is described by a first order ODE, a second order system (modules 3, 4 and 5) by second order ODEs and a system with just a dead time (module 2) is described by an algebraic equation in the time domain. Since our overall model is nonlinear, it is more convenient to express its governing equations in the time domain rather than in the form of transfer functions in the Laplace domain. Let $y_i(t)$ be the output of module i in Figure 7 at time t. Then, for step changes in the LPA, TGF and HGF concentrations to values L, T and H respectively, the change in the system variables $y_i(t)$ over time are described by the following ODEs:

$\tau_1 dy_1/dt + y_1 = 0$ (Module 1)

$$\tau_2\tau_3\, d^2y_3/dt^2 + (\tau_2+\tau_3)\, dy_3/dt + y_3 = K_3\, y_6(t) \qquad \text{(Module 3)}$$

$$\tau_2\tau_3\, d^2y_4/dt^2 + (\tau_2+\tau_3)\, dy_4/dt + y_4 = 0 \qquad \text{(Module 4)}$$

$$\tau_2\tau_3\, d^2y_5/dt^2 + (\tau_2+\tau_3)\, dy_5/dt + y_5 = 0 \qquad \text{(Module 5)}$$

$$dy_8/dt = y_6(t) \qquad \text{(Module 8)} \qquad \text{(S2)}$$

For modules 3-5, which are described by second order ODEs, we need to specify two initial conditions, one for the variable itself, and another for the derivative of the variable. The initial conditions for the ODE system are as follows: $y_1(0) = K_1L/\tau_1$; $dy_4/dt(0) = K_4T/(\tau_2\tau_3)$; $dy_5/dt(0) = K_5H/(\tau_2\tau_3)$; $y_3(0) = dy_3/dt(0) = y_4(0) = y_5(0) = 0$; $y_8(0) = LIG(0)$, the ligand amount measured at time 0 for the control case in Figure 2C.

The above differential equations need to be solved in conjunction with the following algebraic equations:

$$y_2(t) = K_2\, y_7(t - t_d) \qquad \text{(Module 2)}$$

$$y_6(t) = K_6[y_1(t) + y_2(t)] / \{K_{S6} + [y_1(t) + y_2(t)]\} \qquad \text{(Module 6)}$$

$$y_7(t) = K_7\,[y_3(t) + y_4(t) + y_5(t)] / \{K_{S7} + [y_3(t) + y_4(t) + y_5(t)]\} \qquad \text{(Module 7)} \qquad \text{(S3)}$$

Note that in Eq. S2 the input ligand concentrations appear as initial conditions and not in the equations themselves. This is due to the fact that modules 1, 2 and 3 contain an "*s*" term in the numerator, which converts the step input to an impulse. For any given set of input strengths, and parameter values, we solved equations S2 and S3 in MATLAB (Mathworks, Natick, MA) using the delay-differential equation solver *dde23* to obtain the outputs that we are interested in: the level of ERK activation, $y_7(t)$, and the amount of shed ligand, $y_8(t)$.

Parameter estimation

The mathematical model for the transactivation system contains 13 unknown parameters. There are the 9 transfer function parameters for the core LTI modules: K_1 [units: (pg $\times 10^{-2}$ /min) / (μM LPA)] , τ_1 [units: min], K_2 [units: (pg $\times 10^{-2}$ /min) / (ng/ml pERK)] , t_d [units: min], K_3 [units: (ng/ml pERK)/ (pg $\times 10^{-2}$ /min)], τ_2 [units: min], τ_3 [units: min], K_4 [units: (ng/ml pERK)/ (ng/ml TGF)] and K_5 [units: (ng/ml pERK)/ (ng/ml HGF)]. In addition to these, we have a total of 4 parameters in the sigmoidal saturation functions for ligand shedding rate and ERK activation: K_6 [units: (pg $\times 10^{-2}$ /min)], K_{S6} [units: (pg $\times 10^{-2}$ /min)], K_7 [units: (ng/ml)] and K_{S7} [units: (ng/ml)]. Given the values for this entire parameter vector θ, and the input concentrations L (μM), T (ng/ml) and H (ng/ml) we can compute the system response using the equations and initial conditions

presented above. For any given input condition we computed the ERK output at time *t,* as $y_7(t)$; and the shed ligand amount at time *t,* as $y_8(t) + LIG_{control}(t)$. $LIG_{control}(t)$ is the constitutive ligand shedding and was computed by interpolating the data points shown in the control case experiment in Fig. 2A.

The experimental data consists of time course measurements for ERK and shedding at fixed ligand doses, and dose response measurements at fixed times. Say for a particular input-output combination (e.g. input = LPA, output = pERK), the time course is measured at a ligand dose D_e and the dose response is measured at a time point t_e. In order to simultaneously fit the time course and dose response data, we scaled the dose response curve so that the dose response value at time t_e would equal the value determined in the time course experiment for $D=D_e$ and $t=t_e$. In essence, we assume that the shape of the dose response curve is invariant while the values themselves could depend on the cell culture conditions. This is supported by the data shown in Fig. S4. We generated model predictions for pERK and shed ligand at the appropriate dose and time point values dictated by our experimental measurements. We then computed a weighted residual vector $[(Y_{model} - Y_{exp})/ \mathrm{Max}(Y_{exp})]$ for each of the experimentally measured dose response and time course curves. This weighting ensures that all of the curves make comparable contributions to the overall residual during parameter estimation. We then constructed the overall weighted residual vector by combining the residuals for all the experiment curves. This residual vector, $\mathrm{Res}(\theta)$, is a function of the model parameters, θ, and was minimized using the MATLAB nonlinear least squares regression function *lsqnonlin* to obtain estimates for the model parameters. We defined search ranges for each of the parameters (Table S3) and performed 100 optimization iterations starting from random positions within the chosen parameter bounds. The root-mean-squared value of the residual vector (RMSD) was determined for each of these solutions. Parameter sets that yielded an RMSD within 1% of the minimum value were analyzed to determine the uncertainty in the individual parameters (Table S3). We computed the mean, standard deviation, CV, and the 10th, 50th and 90th percentile values for each of the 13 model parameters using all qualifying solutions (Table S3).The best-fit parameter set that resulted in the lowest RMSD was used to obtain the results in Figs. 7 and 8 of the manuscript. Despite the uncertainties in some of the parameters, our predictions for the overall behavior of the transactivation circuit remain unchanged when we use any of the parameter sets that yield a good match between model and experiment (Fig. S7).

Model fits to the experimental data using the best fit parameter set are shown in Fig. S6. Although the model does not perfectly capture each individual time-series or dose response curve, the overall fit is reasonable given the fact that we are simultaneously fitting data from 11 individual experiments using a relatively small set of parameters. The R^2 values (Fig. S6) are acceptable for all of the curves except for the HGF-induced shedding dose response where R^2 = 0.47. This is likely due to using the closed-loop response to three distinct inputs to obtain the parameters for the common positive feedback loop. Our ability to obtain a reasonable fit to the data suggests that the model is internally self-consistent and that each of the three stimuli for the most part activate an invariant feedback loop. The discrepancies in the fit could reflect subtle differences in the manner in which the three inputs engage the autocrine circuit.

Steady-states and system stability

Once, we obtained the parameters of the mathematical model, we performed a steady-state stability analysis to examine the properties of the autocrine feedback loop. Equations S2 and S3 can be used to determine the steady-state level of pERK in the system in response to a perturbation. In our model, the ligand shedding response to LPA, and the ERK activation response to TGF and HGF are each modeled as transients that decay to zero at long enough times (see Table S2). In this scenario, modules 1, 4 and 5 can be ignored in determining the steady-state. Setting the derivatives in the governing equation for module 3 to equal zero and combining the resultant algebraic equation ($y_3^{SS} = K_3 y_6^{SS}$) with the expressions in Eq. S2, yields the following nonlinear differential equation for the system:

$$\tau_2\tau_3\frac{d^2y_3}{dt^2}+\left(\tau_2+\tau_3\right)\frac{dy_3}{dt}+y_3=\frac{K_2K_3K_6K_7y_3}{K_{S6}K_{S7}+\left(K_2K_7+K_{S6}\right)y_3} \qquad \text{(S4)}$$

Setting the derivatives to equal 0 in Eq. S4, allows us to calculate the steady-state values for y_3, which can then be used to compute the steady-state levels for all the other system variables. We find that there are two possible steady-states for y_7 the readout for ERK activation: one at $y_7^{SS} = 0$, and the second given by the following expression:

$$y_7^{SS} = (K_2K_3K_6K_7 - K_{S6}K_{S7})/(K_2K_3K_6 + K_2K_{S7}) \qquad \text{(S5)}$$

For $K_2K_3K_6K_7 < K_{S6}K_{S7}$, we have a single steady-state at $y_7^{SS} = 0$. For $K_2K_3K_6K_7 > K_{S6}K_{S7}$, in addition to the 0 steady-state, the non-zero steady-state given by Eq. S5 would be positive and hence viable. The actual basal state of the system would depend upon the stability of each of these steady-states.

To determine the stability around a steady-state value, we can examine how the linearized version of the model behaves in the vicinity of the steady-state. Linearizing the term in the right hand side of Eq. S3 converts it to a linear ordinary differential equation, which can be used to compute a transfer function. This transfer function describes how the system responds to small perturbations, when it starts from the specified steady-state. For stability, the roots of the terms in the denominator of the transfer function should have negative real parts. Using this requirement, we can show that the steady state at $y_3 = 0$ (and $y_7 = 0$) is only stable if $K_2K_3K_6K_7 < K_{S6}K_{S7}$. Further, the steady-state given by Eq. S5 is only stable if $K_2K_3K_6K_7 > K_{S6}K_{S7}$. These results were used to generate Fig. 8A of the manuscript.

The steady-state analysis indicates that if the feedback in the system is sufficiently strong, the system would prefer the nonzero steady state, and would thus be in a pre-activated basal state prior to ligand addition. For the dynamic simulations shown in Figs. 8B and 8D of the manuscript we used the specified value of K_2, and fixed values for the other system parameters, to compute the system steady-state as described above. This steady-state was used as the initial condition for computing the pERK dynamic response to TGF .

Note that irrespective of the strength of the feedback loop, the autocrine feedback loop has a stable steady-state. Thus, a transient perturbation would result in a transient response that returns to the original steady state value. This is a consequence of the negative mechanisms that turn off ERK signaling. This feature is implicitly encoded in our mathematical model in the form of the assumption that an impulse in the *ligand shedding rate* (a step change in ligand concentration), would result in a transient pERK response. For low, physiological ligand concentrations, this shut off could be due to the removal of the ligand from the extracellular medium via induced receptor trafficking, which results in signal shut off. Further, there are several negative feedback mechanisms that are known to directly modulate the ERK signaling cascade, and these could be responsible for the adaptation in ERK activity in the face of the continued presence of ligand even at high ligand dosages.

Here, we use sigmoidal saturation functions to account for the fact that ERK and shedding are saturable processes. This renders the model more realistic and enables us to generate predictions for inputs and feedback strengths that the model is not explicitly trained on. To examine the role of this nonlinear saturation on the steady-state behavior of the system, we analyzed what would happen without such saturation effects. Exclusion of sigmoidal saturation would still enable us to fit the time course data sets shown in Figs. 2A and 2C. Let us say K_2 and K_3 are the gains for modules 2 and 3 determined by fitting a linear model (same as Fig. 7, but

with modules 6 and 7 eliminated) to the time course data. It can be shown that such a model has a single steady-state value at $y_3 = 0$ irrespective of the strength of the feedback loop. This steady-state would be stable for $K_2K_3 < 1$, and the system would show a transient pERK response to perturbations under these conditions. However for $K_2K_3 > 1$, the steady-state at $y_3 = 0$ would become unstable, and since there is no other stable steady-state, the system would end up yielding maximal values for ERK activation. Such a system would switch to maximal ERK activation as we increase the strength of the feedback loop. Inclusion of nonlinear saturation effects results in a second nonzero steady-state for $K_2K_3K_6K_7 > K_{S6}K_{S7}$. This steady-state (Eq. S5) is a function of the strength of the feedback loop. Thus nonlinear saturation of ERK and shedding results in an ability to tune the basal state of the system in a graded fashion as a function of the strength of the feedback loop (see Fig. 8A).

So far in our analysis we have assumed that TGF and HGF are transient activators of ERK signaling. These transients are captured by modules 4 and 5 in the model respectively. If in addition, to the transient response, TGF and HGF were to generate sustained contributions to ERK activity at the levels y_4^{SS} and y_5^{SS} respectively, then the overall steady-state pERK level, y_7^{SS} in the presence of feedback is given by the solution to the quadratic equation $Ay_7^2 + By_7 + C = 0$, where $A = K_2K_3K_6 + K_2(K_{S7} + y_4^{SS} + y_5^{SS})$; $B = K_{S6}(K_{S7} + y_4^{SS} + y_5^{SS}) - K_2K_3K_6K_7 - K_2K_7(y_4^{SS} + y_5^{SS})$; $C = -K_7K_{S6}(y_4^{SS} + y_5^{SS})$. For Fig. 8D in the manuscript, we independently varied y_4^{SS} and y_5^{SS} and determined the steady-state pERK level, y_7^{SS} in the presence of feedback by solving the above quadratic equation. For all the cases examined a single viable solution was obtained. In the absence of feedback the expected pERK level at steady-state would simply be $y_7^{SS} = y_4^{SS} + y_5^{SS}$ as long as we are below saturation levels for ERK activation.

SUPPLEMENTARY MATERIAL REFERENCES

1. Asthagiri, A.R. & Lauffenburger, D.A. Bioengineering models of cell signaling. *Annual review of biomedical engineering* **2**, 31-53 (2000).
2. Wang, Z. & Zhang, J. In search of the biological significance of modular structures in protein networks. *PLoS computational biology* **3**, e107 (2007).
3. Saez-Rodriguez, J. *et al.* Multistability of signal transduction motifs. *IET systems biology* **2**, 80-93 (2008).
4. Del Vecchio, D., Ninfa, A.J. & Sontag, E.D. Modular cell biology: retroactivity and insulation. *Molecular systems biology* **4**, 161 (2008).

SUPPLEMENTARY TABLE S1

Table S1
Effect of an Inhibitor Panel on ERK phosphorylation

Inhibitor	Target	Dose (μM)	Stimulant		
			LPA	EGF	HGF
PD-153035	EGFR	1.0	+++	+++	-
KN-62	CaMKII	1.0	+	-	++
KN-93	CaMKII	0.4	+	-	-
BAY 11-7082	IKK	20	++	+	-
AG-490	JAK2	0.1	-	-	+
SP 600125	JNK	8.0	+	-	-
PD-98059	MEK	50	+++	+++	+++
U-0126	MEK	10	+++	+++	+++
AG-879	NGFR	10	-	-	-
SB-203580	P38-MAPK	0.03	-	+	-
SB-202190	P38-MAPK	0.05	-	-	-
LY 294002	PI3K	10	++	-	++
Wortmannin	PI3K	0.05	++	+	++
H-89	PKA	0.05	-	-	-
Hypericin	PKC	2.8	-	+	+
Palmitoyl-DL-carnitine Cl	PKC	0.01	-	-	-
PP2	SRC	10	++	-	-

Shown is the degree of inhibition of phospho-ERK levels that was observed following 30 min treatment with the indicated concentration of inhibitors and 10 min stimulation with the indicated agonists. Results are average of duplicate experiments. Phospho-ERK levels were measured using a Luminex assay as described in Methods. "-" indicates no inhibition, "+" indicates ~25% inhibition, "++" indicates ~50% inhibition and "+++" indicates ~100% inhibition. LPA was used at 20μM, EGF at 10ng/ml and HGF at 20ng/ml.

Supplementary Table S2. Chosen TF forms and the rationale for their selection*

Module	TF form	Rationale
Ligand shedding modules:		
Module 1: LPA induced shedding	$G_1(s) = \frac{K_1 s}{(\tau_1 s + 1)}$	Input is a step change in LPA, and the ligand shedding rate after a transient increase decays with time (Fig. 2C). We don't have strong evidence suggesting the presence of a finite response rise time.
Module 2: ERK induced shedding	$G_2(s) = K_2 e^{-t_d s}$	TGFα and HGF induce immediate ERK activation (Fig. 2A), but the ligand shedding shows the presence of a dead-time. No evidence for a decaying response.
ERK activation modules:		
Module 3: Autocrine ligand induced ERK	$G_3(s) = \frac{K_3}{(\tau_2 s + 1)(\tau_3 s + 1)}$	Step changes in TGFα and HGF induce transient ERK activation with a finite rise time (Fig. 2A). G_4 and G_5 were chosen based on this information. ERK activation was assumed to occur with similar dynamics irrespective of the stimulus (TGFα, HGF, autocrine ligand). Hence, the characteristic response times (τ) were assumed to be the same for G_3, G_4 and G_5. The input to module 3 is a shedding rate, which is already a derivative of the ligand concentration. Hence the '*s*' term was dropped from the numerator of G_3.
Module 4: TGFα induced ERK	$G_4(s) = \frac{K_4 s}{(\tau_2 s + 1)(\tau_3 s + 1)}$	
Module 5: HGF induced ERK	$G_5(s) = \frac{K_5 s}{(\tau_2 s + 1)(\tau_3 s + 1)}$	

The TF forms chosen were the simplest possible ones that could explain the qualitative dynamic features of the EGFR transactivation circuit (Fig. 2 in the manuscript). The responses of these TF forms to unit step inputs are presented in Fig. S5.

Supplementary Table S3. Parameter estimates and uncertainty in individual parameters

		Search Range						Percentiles		
Module	**Parameter**	**Min**	**Max**	**Best Fit**	**Mean**	**SD**	**CV**	**10th**	**50th**	**90th**
LPA-induced shedding	K_1 (pg×10^{-2} /min)/(μM LPA)	0.1	100	22.8156	23.4069	6.5749	0.2809	12.9214	23.6821	31.6184
	τ_1 (min)	1	25	1.5834	1.5255	0.108	0.0708	1.3898	1.5234	1.6287
ERK-induced shedding	K_2 (pg×10^{-2} /min)/(ng/ml pERK)	0.01	10	0.0533	0.0571	0.0159	0.278	0.0294	0.0617	0.0704
	t_d (min)	10	30	23.2909	22.6124	0.4696	0.0208	21.9557	22.5914	23.3185
Autocrine ligand-induced ERK	K_3 (ng/ml pERK)/(pg×10^{-2} /min)	0.1	100	5.0012	7.2413	2.1684	0.2994	4.4309	7.9752	9.5871
	τ_2 (min)	0.1	10	0.5017	0.8337	0.3099	0.3717	0.4432	0.7568	1.3043
	τ_3 (min)	5	50	9.3723	9.191	0.3266	0.0355	8.8521	9.239	9.4596
TGF -induced ERK	K_4 (ng/ml pERK)/(ng/ml TGF)	0.1	100	28.4561	39.0561	11.6612	0.2986	23.3459	39.5387	52.2767
HGF-induced ERK	K_5 (ng/ml pERK)/(ng/ml HGF)	0.1	100	11.5128	15.4065	4.4211	0.287	9.2853	16.6236	20.5814
Shedding saturation	K_6 (pg×10^{-2} /min)	0.01	100	0.1809	0.1868	0.0112	0.0602	0.1764	0.1855	0.2031
	K_{S6}/K_6 (dimensionless)	0.001	1	0.6699	0.729	0.2022	0.2774	0.3722	0.7692	0.8946
pERK saturation	K_7 (pg×10^{-2} /min)	0.1	100	0.9766	0.9796	0.0028	0.0028	0.9763	0.9794	0.9835
	K_{S7}/K_7 (dimensionless)	0.001	1	0.4066	0.5752	0.1721	0.2992	0.352	0.6159	0.7642

Parameters were estimated by fitting the model to the experimental data. Bounds were placed on the individual parameters as indicated in the "Search range" columns above. The optimization was run 100 times with initial values randomly chosen within the indicated parameter bounds. The best fit column shows the parameter set that yielded the minimum root-mean-squared deviation (RMSD) between model and experiment. Solutions that had an RMSD value within 1% of the best fit RMSD were used to compute parameter statistics - mean, standard deviation (SD), coefficient of variation (CV), and the 10^{th}, 50^{th} and 90^{th} percentiles. The variability in any given parameter reflects the inability of the model to obtain a unique estimate for its value. Parameters with CV > 0.1 are highlighted in red. Of these, the parameters K_1 and K_2 and K_{S6} form a mutually correlated set, which together determine the magnitude of ligand shedding. Similarly the parameters K_3, K_4, K_5 and KS_7 comprise a correlated set, which together determine the magnitude of ERK activation. These correlations contribute to the uncertainties in these parameters. The uncertainty in τ_2 is due to the lack of sufficient data to accurately estimate the rise time for ERK activation.